IMAGE RECONSTRUCTION USING ELECTRON MICROGRAPHS OF INSECT FLIGHT MUSCLE

Use of Thick Transverse Sections to Supplement Data from Tilted Thin Longitudinal Sections

KENNETH A. TAYLOR, MARY C. REEDY, LEONIDAS CORDOVA, AND MICHAEL K. REEDY
Duke University Medical Center, Department of Anatomy, Durham, North Carolina 27710

ABSTRACT Three-dimensional reconstruction using electron micrographs of thin sections is a powerful technique for determining cross-bridge structure. Tilt restrictions in the electron microscope prevent data collection beyond tilt angles of 60°, giving rise to a "missing cone" of transform data. We show here how much of this data can be obtained using micrographs of thick transverse sections, and the effect this data has on reconstructed images of the insect flight muscle MYAC layer. As a byproduct, the analysis showed that section thinning resulting from prolonged electron irradiation had occurred in the thin longitudinal section used for the previously published MYAC layer reconstruction (Taylor et al., 1984). Comparison of projection density maps calculated from the thin longitudinal section reconstruction and the thick section data show that the data within the missing cone that is not accessible by tilting sharpens the boundaries of the components, flattens the density profile across the thick filament, and enlarges the molecular envelope of the thin filament. We conclude that the reconstructed images of the MYAC layer provide a picture of the structural principles underlying the system but that transform data within the missing cone are necessary to describe accurately the envelopes and profiles of these structural elements.

INTRODUCTION

The study of the structural intermediates in muscle contraction has involved the combined approaches of x-ray diffraction (Holmes et al., 1980; Huxley et al., 1983; Brenner et al., 1984), electron spin resonance (Thomas and Cook, 1980; Thomas et al., 1983), biochemical probes (Lovell et al., 1981; Yanagada, 1981) and electron microscopic techniques (Reedy et al., 1965; Heuser, 1983; Reedy et al., 1983*b*). Each method possesses its own set of advantages and disadvantages. For instance, x-ray diffraction offers the opportunity to study live muscle and to investigate the structural changes that occur during muscle contraction through the use of time-resolved diffraction methods. However, the phasing problem makes difficult the transition from diffraction data to a specific structure. Biochemical probes and ESR techniques can report site-specific changes occurring during contraction, but cannot provide an image of the intermediate states.

Electron microscopy and particularly the technique of three-dimensional image reconstruction applied to electron micrographs has played an important role in the study of muscle structure. Studies of numerous filamentous aggregates such as F-actin (Moore et al., 1970; Wakabayashi et al., 1975; Smith et al., 1984), the F-actin-Myosin subfragment 1 complex (Taylor and Amos, 1981; Vibert and Craig, 1982; Toyoshima and Wakabayashi, 1985), and thick filaments from several muscle systems (Vibert and Craig, 1983; Stewart et al., 1985) have done much to extend our knowledge of some of the isolated components of the muscle. More recently, the structure of the filament lattice of several muscle types has been examined by three-dimensional reconstruction techniques of thin sections. In addition to the insect flight muscle under discussion here, the fish muscle M-band has been reconstructed using multiple tilt views (Luther and Crowther, 1984) as well as the recent oblique section reconstruction technique (Crowther and Luther, 1984). The application of three-dimensional reconstruction to sectioned muscle offers the opportunity to extend our knowledge of the structure of its various components to the intact system.

Electron microscopy suffers from the disadvantage that tissue must be processed for examination by a series of chemical treatments that may lead to alterations in the native structure. Such changes can be minimized through x-ray monitoring of tissue preparation procedures to select protocols that retain most faithfully the diffraction features of the native muscle (Reedy et al., 1983*a*). The goal of the microscopist, therefore, is to derive structural principles for the spatial organization of the muscle components as well as models for the cross-bridge states that can be tested in native muscle by other means, such as by x-ray diffraction.

A potentially exciting area for three-dimensional reconstruction is the investigation of different static states which may represent intermediates in the contraction cycle. Currently accessible static states include rigor, in which cross-bridges are attached to actin in a form believed to represent the end of the force-generating step, and the relaxed state in which cross-bridges are detached from actin and poised at the beginning of the cross-bridge cycle. Nucleotide analogue states such as that induced with AMPPNP may correspond to attached cross-bridge states which occur during force generation (Goody et al., 1975).

Of all the muscle types available, the asynchronous flight muscles of the waterbug *Lethocerus* are the most highly ordered and thus make an ideal material for study by both x-ray diffraction and electron microscopy. We recently began a study of the structure of the accessible static states of this muscle by three-dimensional image reconstruction of thin sections of fixed and embedded tissue using the tilt view reconstruction method of Henderson and Unwin (1975). A particularly useful class of specimens for this purpose is the MYAC layer, composed of alternating thick and thin filaments in a thin longitudinal section 20–25 nm thick. Our recent work (Taylor et al., 1984; Reedy and Reedy, 1985) on the three-dimensional structure of the rigor MYAC layer made three important observations. First, two forms of averaged rigor cross-bridges were observed that differ from each other in density (presumed to indicate one-headed vs. two-headed bridges), in their angle of tilt with respect to the filament axis, and in the shape and azimuth of the portion of the cross-bridge proximal to the thick filament. Second, the two long-pitch helical strands of the actin-containing thin filament were resolved and confirmed the geometry of cross-bridge binding to actin of Taylor and Amos (1981). Third, periodic changes in the twist and strand separation of the actin helix were observed in association with alternation of one-headed and two-headed cross-bridges binding to a single thin filament.

One technical limitation of the tilt view reconstruction method is the restriction to only 60° of tilt, which leaves inaccessible a "missing cone" containing some 13% of the transform data from a two-dimensional crystalline array. Of particular importance is the missing data along the ($0,0,Z^*$) lattice line which contains the information on the density profile normal to the plane of the section. These data are particularly important for sharpening the features at the boundaries of the section, and for determining the actual thickness of the section. Thin-sectioned single filament arrays of insect flight muscle have a richly detailed equatorial diffraction pattern. In principle, the same data can be obtained from individual rows of filaments viewed end-on in a thick transverse section. We have therefore compared both types of data to evaluate the magnitude and structural significance of that region of the transform missed in one type due to the tilting restrictions. This should have been a somewhat pedestrian exercise but produced the unexpected observation that the thin section used in our previously published MYAC layer reconstruction had suffered a considerable amount of mass loss prior to data collection. The work also illustrates what effect this missing cone data and especially the density profile across the section thickness can have on reconstructed images of muscle.

METHODS

Electron Microscopy

Glycerinated dorsal longitudinal flight muscles from the waterbug *Lethocerus* were prepared by fixation in 0.2% tannic-acid, 2.5% glutaraldehyde in 20 mM MOPS + 10 mM $MgCl_2$ at pH 6.8, followed by cold 1.0% OsO4 in 0.1M P04 buffer plus 10 mM $MgCl_2$ at pH 6.0. Tissue was block-stained in 1% aqueous uranyl acetate, dehydrated in ethanol, and embedded in Araldite 506. Sections were stained by the permanganate-lead sequence (Reedy, 1968; Reedy et al., 1983*b*). Thin (25 nm) longitudinal sections and thick (110 nm) transverse sections were cut from the same fiber bundle with a diamond knife (Diatome, Port Washington PA) on a Reichert OMU-3 Ultramicrotome.

Electron micrographs for the tilt series reconstruction were taken on a Philips EM 400 electron microscope equipped with 60° goniometer stage (Philips Electronic Instruments, Mahwah, NJ). Micrographs of thick transverse sections were taken on a Philips EM 300.

Image Processing

Tilt View MYAC Layer Reconstruction. Transform data for the three-dimensional reconstruction of the longitudinal thin section MYAC layer were obtained by Fourier transformation of digitized electron micrographs which were recorded at a magnification of 17000× and digitized using a pixel size of 1.7 nm with respect to the original specimen (Taylor et al., 1984). Arrays for Fourier transforms were 256 × 256 in size. Structure factor data from two orthogonal tilt series of a single MYAC layer were combined in the two-sided plane group p12. Because this procedure samples the continuous transform along the individual lattice lines at irregular intervals, smooth curves were drawn by hand through amplitude and phase plots of the merged data and were sampled at regular intervals of 0.01 nm^{-1} to form the data set used for subsequent comparison with the thick section data. Data analysis for this aspect of the work was done on the IBM 3081 computer at the Triangle Universities Computation Center, Research Triangle Park, NC.

Thick Transverse Section Analysis. MYAC rows consist of alternating thick and thin filaments viewed end-on in thick transverse sections. Transform data for four neighboring MYAC rows were obtained from an area of the electron micrograph that produced particularly sharp diffraction, equivalent in resolution to eight orders of the 55 nm interfilament repeat spacing (Fig. 1). Within the selected area, filament profiles were circular and 24–26 nm across. The image was digitized using a Perkin-Elmer PDS1010M microdensitometer at a raster size of 1 nm

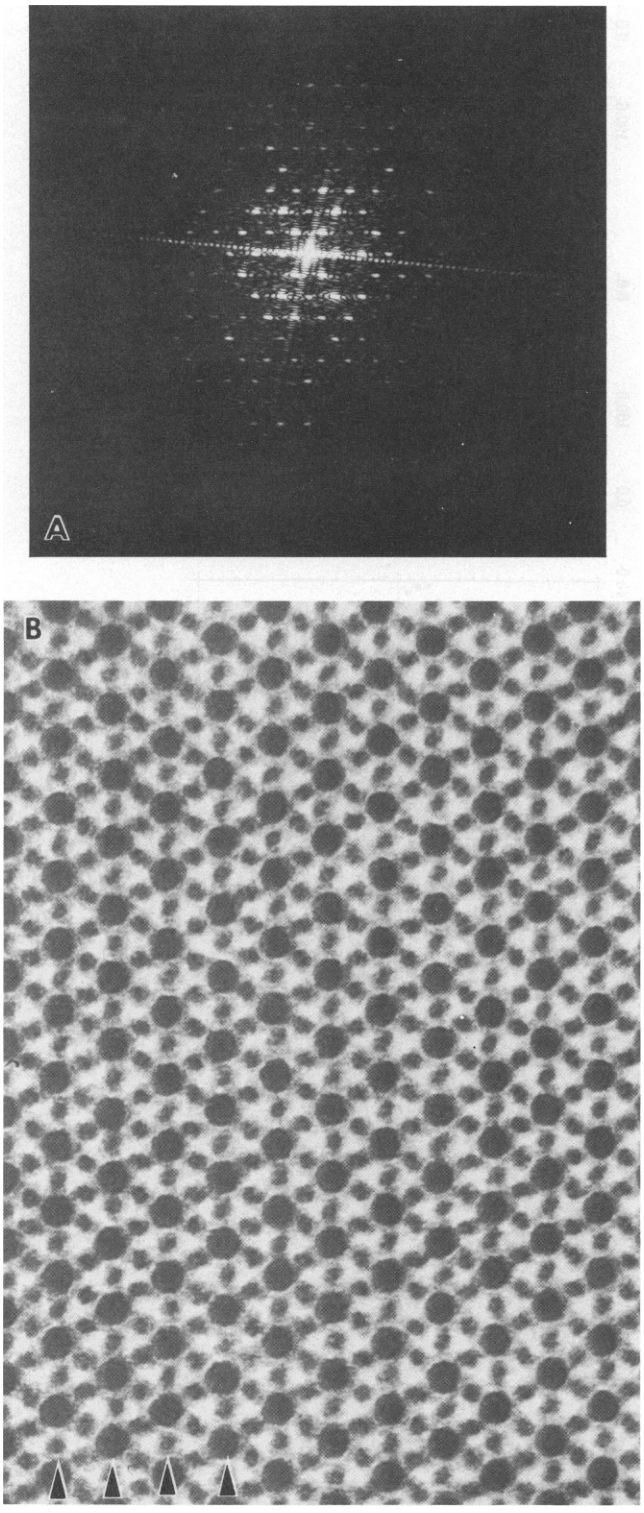

FIGURE 1 Electron micrograph of a thick transverse section of insect flight muscle (*A*) and its optical diffraction pattern (*B*). This diffraction pattern is oriented correctly with respect to the image shown in *A*. The four MYAC rows that were processed are marked with triangles in (*B*). Each was ~9 interfilament repeats long. Magnification 150,000×.

with respect to the original object. Amplitudes and phases along nine lattice lines including the $(0,0,Z^*)$ lattice line were interpolated from 512 × 1024 Fourier transform arrays at intervals of 0.01 nm^{-1}. MYAC rows were 24 pixels wide corresponding to a width of 24 nm. Image densities were floated prior to transformation to minimize the effect of the box transform. The four data sets were averaged together to reduce noise and to give some measure of the reproducibility of the data along each lattice line. Phase residuals obtained in correlations between the four MYAC row data sets and their average ranged between 13.2° and 19.7° with no Z^*-scaling required to obtain good fits.

The $(H,0,Z^*)$ lattice lines obtained by averaging the four MYAC row data sets from the thick transverse section were cross-correlated with the averaged data derived from the tilted thin section. In this correlation procedure the phase residuals were amplitude weighted. In addition to refining the origin along X (the interfilament direction) and Z (the direction normal to the plane of the longitudinal section), the scaling of lattice line data along Z^* was also provided for. Finally, the averaged MYAC row data was phase-origin–shifted, and individual lattice lines were amplitude-weighted and Z^*-scaled to form the data set plotted in Fig. 2 and used for map calculations in Fig. 4. Although amplitude-weighting was done individually for each lattice line, Z^*-scaling was identical for each.

RESULTS

Cross Correlation and Scaling

The three-dimensional Fourier transform of a two-dimensional crystal consists of a series of lattice lines oriented normal to the plane of the crystal and arranged in a regular array defined by the in-plane unit cell constants. The transform itself along each lattice line is unsampled. The tilt view reconstruction method samples this continuous transform at intervals that are defined by the tilt angle and the orientation of the tilt axis with respect to the in-plane crystalline repeat. This sampling occurs at irregular intervals and is generally restricted in overall distribution by the 60° tilt limit of the electron microscope. An important problem that repeatedly occurs in the reconstruction process is the determination of transform data within this "missing cone", especially the data from the section profile.

For the type of specimen we are dealing with here, some of this missing data can be derived from analysis of images of thick transverse and longitudinal sections. Formally, transform data obtained from a MYAC row as seen in thick transverse section is equivalent to what would be obtained if a thin longitudinal section of a MYAC single filament layer could be tilted to 90° about an in-plane axis perpendicular to the filament axis. Thus, in addition to the structure factor data along the $(0,0,Z^*)$ lattice line, addi-

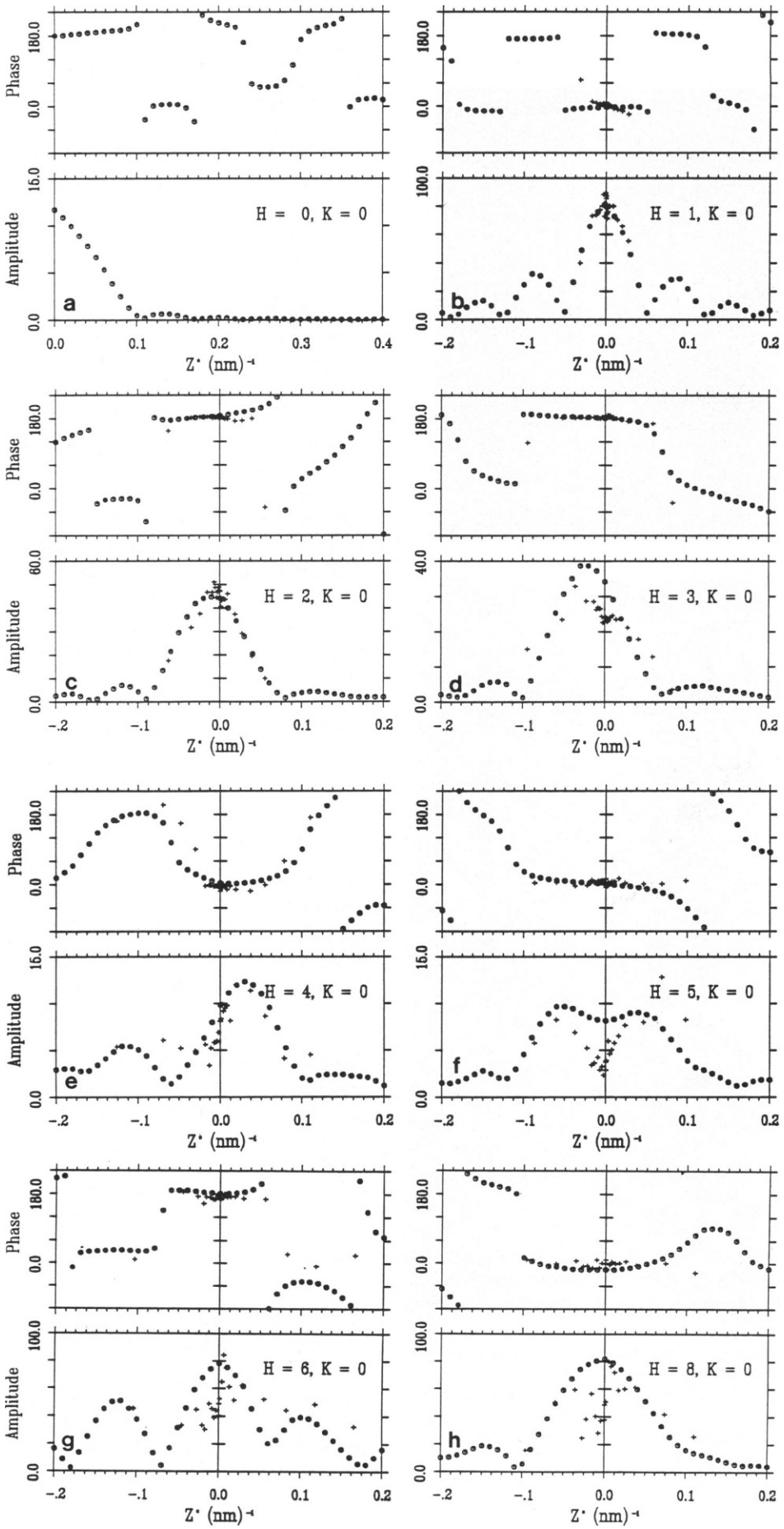

FIGURE 2 Plots of amplitudes and phases of equatorial data derived from thick transverse sections and multiple tilt views of a thin longitudinal section. (*a*) (*0,0,Z**) lattice line. "0"-averaged data derived from the thick transverse section. "+" represents data derived from multiple tilt views. (*b–h*) are the seven lattice lines common to both transverse and longitudinal section data sets.

tional data within the "missing cone" along each of the other eight lattice lines can also in principle be obtained.

One important consideration in the comparison of transform data from a thick transverse section with that from a thin longitudinal section is the relative scaling of the section thickness with the width of the box that is used for limiting the end-on view from the thick section. The exact thickness of a MYAC layer thin section is not usually determinable from the micrograph itself unless a nearby fold is present. Section appearances, as related to the organization of the filament lattice indicated that the range of thickness lay between 20 and 25 nm. Density maps calculated from the thin longitudinal section MYAC layer three-dimensional reconstruction suggested a thickness of ~24 nm but that result could be uncertain because of the lack of transform data along the (*0,0,Z**) lattice line. That value was nevertheless the only basis we had for choosing a box width for MYAC rows. To allow for differences in plate magnification and for real differences in section thickness, the two data sets were cross-correlated using different degrees of Z^*-scaling.

The scaling of transform data along Z^* was critical to the correlation procedure. The computed phase residuals were not, however, an infallible guide for selecting the best Z^*-scaling factor for an optimal fit. This was due to the limited amount of data available on the inner lattice lines from the tilt-view reconstruction, which meant that the phase residuals became insensitive to Z^*-scaling over fairly broad ranges. Phase residuals were consistently poor at Z^*-scaling factors of <1.5, were essentially unchanged between 1.5 and 1.62, and deceptively good above 1.62. We therefore relied on visual comparisons (Fig. 2) of the two types of data to select the best Z^*-scaling within the range of best fits suggested by the computed phase residuals. The surprisingly high value of 1.5 gave best fit as judged by the alignment of the amplitude and phase curves (Fig. 2). The overall phase residual was 19° for what was judged to be the best set of values for X, Z, and Z^*-scale factors.

In addition to allowing for different scaling along Z^*, variations in amplitude of the same lattice line between the two data sets were also observed. It was found that the scale factors that would place the amplitude of each lattice line from the MYAC row data on the same scale as the MYAC layer data were somewhat dependent on resolution (Table I) to the extent that the amplitude-scale factor for the (*8,0,Z**) lattice line was 2.1 times that required for the (*1,0,Z**) lattice line. Intervening lattice lines followed a nearly smooth gradient between the two extremes. This type of systematic difference of amplitude with resolution is very much like what we would expect for relatively greater filament disorder in MYAC row than in MYAC layer data. The differences in amplitude observed between the two set of lattice line data could also result from real differences in degree of staining between the two section types. In placing the MYAC row data onto the same amplitude scale as the MYAC layer data, we therefore

TABLE I
FACTORS DERIVED FOR SCALING AMPLITUDES OF MYAC ROW DATA TO MYAC LAYER DATA

Lattice line		Resolution $(nm)^{-1}$	Scale factor
1	0	0.01694	0.00628
2	0	0.0339	0.00962
3	0	0.05082	0.00976
4	0	0.06776	0.0120
5	0	0.0847	0.0109
6	0	0.10164	0.0126
8	0	0.1355	0.0133

Note that the low value for the scale factor is in large part due to the difference in size of image arrays processed and the different densitometers used for digitizing the two sets of data.

decided not to use a single weighting factor for the entire data set, but rather each lattice line was amplitude weighted individually. We felt that this was justified because the object of this exercise was to evaluate the effect of the missing cone data from the MYAC layer by using the MYAC row transform as a vehicle for extrapolation. Moreover, there was nearly as large a variation in scale factors among lattice lines of the four MYAC row data sets and their average (which was created using uniform weighting factors) as was found between the averaged MYAC row and the MYAC layer data. By weighting the lattice line amplitudes individually the differences in staining and disorder between the two data types may be somewhat compensated. The (*0,0,Z**) lattice line, for which there was no data common to the transverse and longitudinal section data sets, was weighted by the same factor used for the (*1,0,Z**) line.

The agreement between the averaged (*H,0,Z**) lattice lines derived by the above procedure and the comparable data obtained from tilted thin sections was surprisingly detailed (Fig. 2). For example, the maximum amplitude in the (*3,0,Z**) was at $Z^* = -0.025$ nm^{-1} in both data sets, and a pair of asymmetric peaks located at $Z^* = 0.025$ nm^{-1} and -0.08 nm^{-1} in the (*4,0,Z**) lattice line from the MYAC layer transform compares with $Z^* = 0.025$ nm^{-1} and -0.1 nm^{-1} in the MYAC row data. The major differences seem to be confined to the (*5,0,Z**) which had two asymmetric peaks centered at $Z^* = \pm 0.025$ nm^{-1} with a fairly deep minimum between them in the MYAC layer data but had two somewhat symmetric peaks with a shallower minimum at about the same location in the MYAC row data. For eight of the nine lattice lines analyzed, most of the amplitude is contained within $-0.2 < Z^* < 0.2$ nm^{-1}. The very intense (*1,0,Z**) lattice line had numerous subsidiary maxima extending out as far as 0.4 nm^{-1}. The (*7,0,Z**) lattice line was absent in the MYAC layer transform and weak in the MYAC row data set. The weakness of the data beyond 0.1 nm^{-1} in most of the lattice lines represents essentially the effect of convoluting the masking function with the molecular transform of the filament lattice. Reproducible phases were as a rule

obtained out to 0.2 nm^{-1} on most of the lattice lines despite the weakness in amplitude. The multiple tilt procedure therefore determines nearly all of the strong diffraction data along (H,0,Z^*) with the exception of (0,0,Z^*) and some inner subsidiary maxima along the (1,0,Z^*) lattice line.

Comparison of Calculated Density Maps

Density maps equivalent to projections down the filament axis were calculated to compare the different data sets. The density map calculated for the averaged MYAC row lattice lines before the application of any amplitude weighting and Z^*-scaling provides a good baseline for the effects of the various processing procedures on the reconstructed image (Fig. 3). In the unsymmetrized density map (Fig. 3 *a*) the originally 24–26 nm diam circular thick filament profile has been somewhat flattened by the 24 nm-wide box function. The projected density at the thin filament is elongated and skewed 30° from the interfilament axis. The actin dyads are not as pronounced as in the MYAC layer reconstruction, an observation that could be explained by build-up of tannic acid on the thin filament thereby reducing the contrast between the two actin long-pitch strands. Their presence is implied by the elongated shape of the actin density feature which would otherwise be expected to be circular in projection. Note that the expected 20 nm thick filament profile also appears broadened by build-up of tannic acid. The slight asymmetry in the elliptical profile seen at the actin position may be caused by some slight misalignment of the thin filaments to one side, as can be seen in the original micrograph (Fig. 1 *b*). Overall, the density map of the averaged MYAC row lattice line data is faithful to the original micrograph details. Enforcing the twofold rotation axis (Fig. 3 *b*) does little to alter the elongated shape of the density at the actin position or the density profile across the thick filament (which is rather flat in both cases). Its major effect is to divide the single off-centered density in Fig. 3 *a* into two smaller densities.

The density map calculated from the MYAC layer data alone shows clearly a density pair at the actin position that we associate with the two long pitch actin strands (Fig. 4 *a*). These densities do not arise simply by enforcing twofold rotation symmetry on an actin filament that is displaced from its crystallographic position, because the two separated strands can in fact be seen in unprocessed MYAC layer images (Reedy and Reedy, 1985). The projected density expected for an actin filament is a

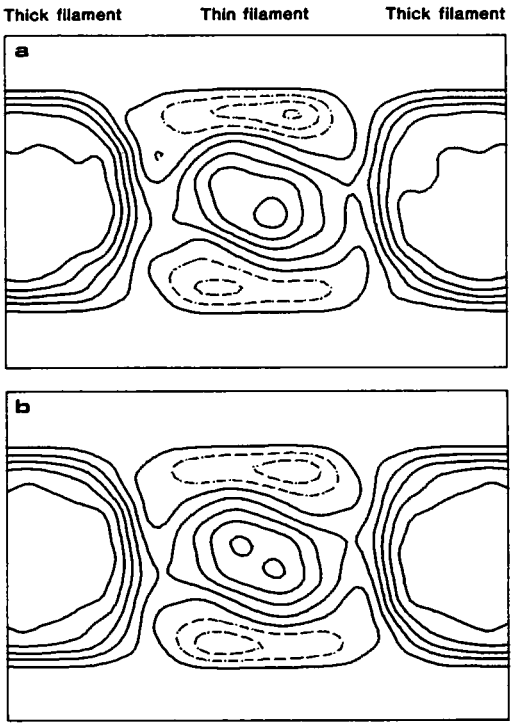

FIGURE 3 Projected density maps of the averaged MYAC row data. These are maps of the original data calculated using an interfilament spacing of 55 nm and a resolution cutoff along Z^* of 0.2 nm^{-1}. Thin dashed lines represent positive densities, presumably regions that project primarily through embedding medium. Solid lines are densities ≤ 0.0 and represent protein regions. (*a*) Unsymmetrized density map. (*b*) Twofold symmetrized map of MYAC row, unscaled and unweighted. Map scale 1.21 mm/nm.

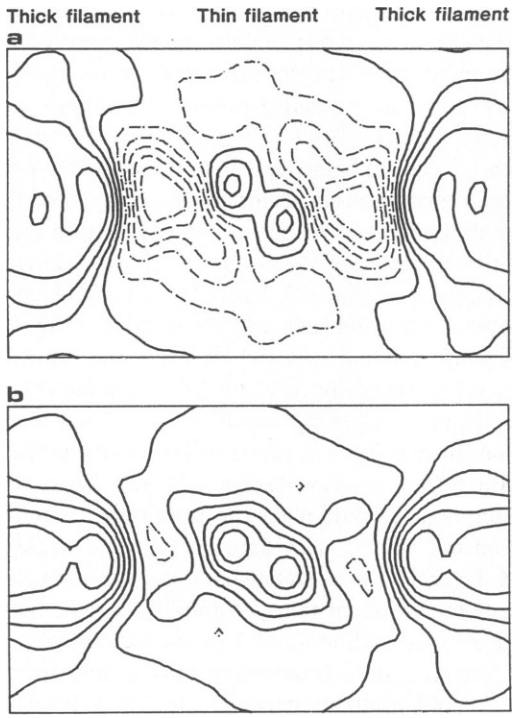

FIGURE 4 Density maps calculated in space group p 12 (i.e., twofold symmetry enforced) of projections down the filament axis from multiple views of a thin section MYAC layer. Maps were calculated using data limited to <0.2 nm^{-1} resolution and using an interfilament spacing of 46.6 nm. (*a*) Projection down the filament axis from just the original MYAC layer data. (*b*) Projection map calculated from the data used in (*a*) plus the (0,0,Z^*) data derived by Z^* scaling and amplitude weighting from the thick transverse section MYAC row (original plus "missing core" data, p 12 symmetrized). Map scale 1.43 mm/nm.

circular profile of ~10 nm diameter (Egelman and Padron, 1984). The presence of two densities in our rigor specimens at the thin filament position arises because the actin filament helix is partly untwisted along half of each 38.7 nm axial repeat period (Taylor et al., 1984); the two straightened strands project as a density pair. These densities are rotated ~30° relative to the interfilament axis and have a center-to-center separation of 6.0 nm. The thick filaments are ~20–21 nm wide along the MYAC layer plane and 24–25 nm thick normal to the MYAC layer plane.

For comparison a projection map was calculated using just data from those MYAC row lattice lines also found in the MYAC layer reconstruction (Fig. 5 *a*). The map is very similar indeed to that obtained from the MYAC layer. The projected density map shows a circular thick filament profile 20 nm in diameter (at the second contour level) and two well resolved actin peaks with a center-to-center separation of 6.3 nm. The density at the actin position is, however, lower than in the projection of the MYAC layer reconstruction.

A density map calculated to a resolution of 0.2 nm^{-1} using all the lattice lines obtained for the MYAC row shows all the density features confined within a band 18 nm thick (Fig. 5 *b*). The center-to-center separation between the density pair at the actin position has been reduced to 4.6 nm. The somewhat rectangular bilobed dense mass at the actin position seen in this map is a better representation of the electron micrograph appearance than the sharply resolved pair of 5 nm densities seen in Figs. 4 *a* and 5 *a*. The thick filament profile is elliptical with dimensions 18.0 nm thick by 22.7 nm wide (measured at the second contour level).

Most of the differences between the maps shown in Figs. 4 *a* and 5 *a* as compared with Fig. 5 *b* are due to the presence of the (*0,0,Z**) data in the latter map. Addition of the (*0,0,Z**) data from the MYAC row to the MYAC layer data set results in a map (Fig. 4 *b*) that is surprisingly similar to that in Fig. 5 *b*. The general similarity of the actin density in Fig. 4 *b* to that seen in the MYAC row reconstruction (Fig. 5 *b*) as well as the micrograph itself (Fig. 1 *b*) suggests that the two actin densities seen in the unmodified MYAC layer reconstruction, although expressing the underlying structural features of the actin filament, do not give an accurate overall description of the envelope of the actin filament in these specimens. It can therefore be concluded that the effect of the lattice line data from the thick transverse section has sharpened the boundaries of the section, evened out the density profile across the thick filament, and raised the density at the actin position. It has had the additional effect of pulling the centers of mass of the actin strands closer together.

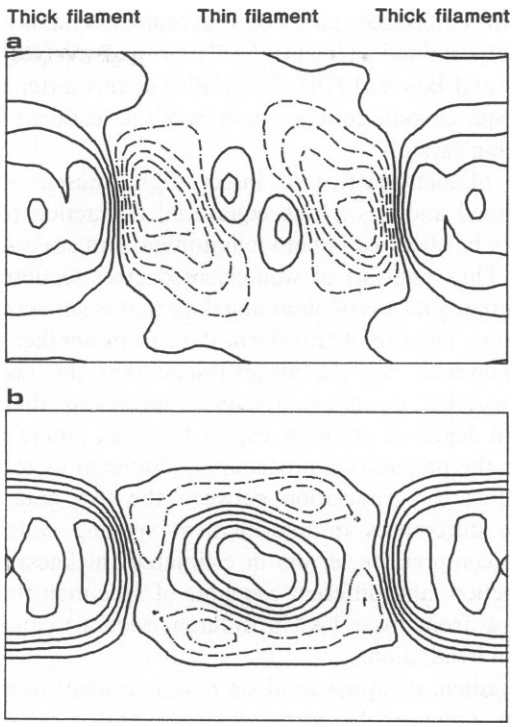

FIGURE 5 Projection density maps calculated from averaged MYAC rows taken from thick transverse sections. (*a*) Map calculated using only those parts of the transform that are also observed in the MYAC layer data (from lattice lines common to the MYAC layer, i.e., without the (*0,0,Z**) lattice line). (*b*) Map calculated using all of the transform data out to a resolution cutoff of 0.2 nm^{-1} and using an interfilament spacing of 46.6 nm. Maps calculated with data to 0.4 nm^{-1} are very similar to that shown in (*b*). Map scale 1.43 mm/nm.

DISCUSSION

Three-dimensional image reconstruction of highly ordered thin sections of insect flight muscle is a powerful technique for determining cross-bridge structure. The application of the technique to sectioned muscle is somewhat difficult because special care must be taken to select areas that are homogeneous and centered, especially if symmetry elements are to be preserved. Sectioning can distort the specimen, altering the interfilament spacing and in general disturbing the nominally hexagonal lattice of the filaments. Section thickness, which is fairly constant over the area of interest, can, however, vary from section to section. For the most part one wishes to obtain most of the reconstruction data from a single area. However, since data from the "missing cone" accessed between 60° and 90° of tilt is practically difficult or impossible to get from just one section, the important density profile across the section thickness must be determined by other means.

Various methods have been used to overcome the tilt restriction of the electron microscope and reduce the amount of data missing in the reconstructions. A favorite method is bending the specimen grid which can enable tilt data to be collected to as high as 75° (Unwin and Zampighi, 1980; Deatherage et al., 1982). Such a procedure is technically unfeasible with sectioned muscle. Profile data has been collected from folds in negatively stained crystals (Unwin and Zampighi, 1980; Smith et al., 1983)

or from embedded and cross-sectioned crystals either positively stained (Unwin, 1977) or negatively stained (Amos and Baker, 1979). The utility of this latter procedure requires some common data from the sections and the tilted thin crystals.

The filament lattice of insect flight muscle is well understood and has a rich equatorial diffraction pattern that can be observed in both longitudinal and cross-section views. Thus analysis of well-oriented cross-sections provides a ready means of obtaining data that is not accessible by tilting. The use of transform data from another specimen, however, has the disadvantage that the resulting reconstruction is an average over specimens that may differ in degree of staining, especially when tannic acid is used in the preparation procedure. Additional factors that can affect the correlation between the two data types include differences in interfilament spacing caused by section compression, errors in estimated thickness of the thin section, and different amounts of specimen thinning resulting from mass loss in different sections caused by electron irradiation.

A gradient of tannic acid staining is evident in muscle bundles prepared by our technique. This ranges from fibrils with a dense coating of stain around each filament and cross-bridge (usually found close to the surface of the bundle), to lighter, positively stained fibers (deeper in the bundle). The measured filament diameter in the published three-dimensional map (Taylor et al., 1984) and in 15-nm transverse sections (Reedy and Reedy, 1985) was 19–22 nm, while the diameter in projection of the thick filament in the 100 nm transverse section used here is ~24–26 nm. This might indicate different degrees of tannic acid build-up in the two sections. It is difficult to appraise relatively small differences in tannic acid build-up in a thick cross-section. We will need to extend our experiment to obviously different parts of the stain gradient before we can better evaluate this factor. (A more heavily stained thick cross-section that was tried initially in this study had a transform that differed unacceptably from the MYAC layer data.)

Also of concern in the integration of the two types of lattice line data is the effect of the prolonged electron exposure required to collect sufficient tilt data from the thin longitudinal section. Previous work with sectioned material embedded in Araldite showed that sections were reduced in thickness by ~50% (Bennett, 1974). In a more recent three-dimensional reconstruction of the fish muscle M-band (Luther and Crowther, 1984), the resulting structure also appeared some 50% thinner than predicted. The lattice line data obtained in this study from thick transverse sections required scaling along the Z^* direction by +50% to produce good fits with similar data derived from thin longitudinal sections. If the Z^*-scaling factor of 1.5 were required solely to compensate for reduction in section thickness caused by electron irradiation, this reduction must amount to 33% of the starting thickness.

One explanation for the thinner-than–expected section might be that the MYAC layer chosen for the multiple tilt view reconstruction was actually 16 nm thick instead of the 24 nm estimated and used in processing the MYAC row. However, in our experience 16-nm thick MYAC layers differ so obviously in appearance from 20–24-nm thick sections that we are certain that the sections studied by multiple tilt views were at least 20 nm thick. Moreover, the three-dimensional density map calculated from the MYAC layer data did show short cross-bridge stumps projecting vertically between the thick filament and the section surfaces (Taylor et al., 1984). These features would be shaved off in sections thinner than 22 nm.

Thick Araldite sections of muscle stained by our procedure show very little beam-induced thinning. In 100-nm thick longitudinal sections, the easily recognized 10.0 planes remain separated by 60° (±4°) during prolonged irradiation, as judged by tilt observations of longitudinal sections of both insect and vertebrate muscle (Reedy, unpublished results). In thin sections, electron beam-induced mass loss was measured directly on embedded sections of insect flight muscle with the aid of electron energy loss spectroscopy (Kopf, Reedy and Taylor, unpublished results). The mass loss demonstrated by this technique was between 30 and 40% after doses of the order 10,000 e^-/nm^2 and remained essentially unchanged at higher doses. Specimen exposures of this order had probably been accumulated before the first micrograph in the tilt series had been taken. If this amount of mass loss manifests itself in an equivalent amount of section thinning, it could account completely for the Z^*-scale factor of 1.5.

The three-dimensional density calculated from just the tilt view reconstruction suggested a section thickness of 22–24 nm. But that map was calculated without the important $(0,0,Z^*)$ data that provide the density profile across the section. The effect of this density profile on the apparent thickness of reconstructed sections is illustrated by comparing Figs. 5 *a* and 5 *b*. The projection density map calculated from the MYAC row data, but edited to include only the data held in common with MYAC layer tilt view reconstruction, displays an apparent section thickness of 22–26 nm (Fig. 5 *a*). The projection map calculated from the complete MYAC row data set (Fig. 5 *b*) displays a section thickness of only 17.5 nm; supplementing the original MYAC layer reconstruction (Fig. 4 *a*) with the profile data has a similar effect (Fig. 4 *b*). This suggests that the structures included in 22-nm sections collapse because of loss of volatile components during initial exposure to the electron beam. Once this initial mass loss occurs, the process stabilizes (mass loss does not continue until the section disappears). Structures included in the thickness of the original section are not removed during irradiation, but are somewhat compacted or collapsed. A lesser degree of thinning for thick sections may indicate stabilization after a relatively smaller mass loss.

Two other related problems with the data from thick sections deserve consideration. At specimen thicknesses in

excess of 120 nm, multiple scattering becomes a serious problem. Implied in all of the reconstruction work reported here is that the image is formed by electrons that have been scattered only once. Multiple scattering events that have caused departures in the image from that predicted for single scattering will have to be evaluated separately. In addition, insect flight muscle has a 38.7 nm axial repeat period. Thus, the number of axial repeat periods contained in a thick transverse section is small (i.e., <4) and is typically nonintegral. This could cause some features in the projection to be emphasized inappropriately.

Several more studies need to be done. Data from thick longitudinal sections, formally equivalent to views of single filament layers tilted to 90° about the filament axis, will be evaluated and can give an independent measure of section thinning as well as filling in the missing cone data along $(0,K,Z^*)$ lattice lines. Finally, the effect of this additional data on the full three-dimensional reconstruction will be evaluated. Our conclusion is that lattice line data from thick sections is easily obtained and can be integrated with three-dimensional transform data from multiple-tilt views.

We have shown here that the effect of adding part of the missing-cone data to muscle reconstructions is to sharpen the boundaries of the section, flatten the profile across the thick filament backbone, and produce a more realistic envelope for the actin filament. We would conclude that the reconstruction done using only the data from the tilted thin section is expressing the underlying features of the structure, but gives a somewhat inaccurate density envelope for some of the features. The supplementation of multiple-tilt view reconstructions with data from orthogonally oriented thick sections will provide somewhat more accurate description of the density distribution within the structure and perhaps lead to a model that is more testable against the x-ray diagram of the native muscle.

This research was supported by National Institutes of Health grants GM 30598 and AM 14317. K. A. Taylor is an Established Investigator of the American Heart Association. Also supported in part by NIH grants 1-S10-RR02283 and 1-S10-RR01932, National Science Foundation grant PCM-8306638, and a Research Gift from the R. J. Reynolds Industries, Inc.

Received for publication 15 May 1985 and in revised form 28 June 1985.

REFERENCES

Amos, L. A., and T. S. Baker. 1979. Three-dimensional image of micrographs. *Int. J. Biolog. Macromolec.* 1:146–156.

Bennett, P. M. 1974. Decrease in section thickness on exposure to the electron beam; the use of tilted sections in estimating the amount of shrinkage. *J. Cell Sci.* 15:693–701.

Brenner, B., L. C. Yu, and R. J. Podolsky. 1984. X-ray diffraction evidence for cross-bridge formation in relaxed muscle fibers at various ionic strengths. *Biophys. J.* 46:299–306.

Crowther, R. A., and P. K. Luther. 1984. Three-dimensional reconstruction from a single oblique section of fish muscle M-band. *Nature* (*Lond.*). 307:569–570.

Crowther, R. A., R. Padron, and R. Craig. 1985. Three-dimensional structure of tarantula thick filaments. *J. Mol. Biol.* In press.

Deatherage, J. F., K. A. Taylor, and L. A. Amos. 1983. Three-dimensional arrangement of the cell wall protein of *Sulfolobus acidocaldarius*. *J. Mol. Biol.* 167:823–848.

Egelman, E. H., and R. Padron. 1984. X-ray diffraction evidence that actin is a 100 Å filament. *Nature* (*Lond.*). 307:56–58.

Goody, R. S., K. C. Holmes, H. G. Mannherz, J. Barrington Leigh, and, G. Rosenbaum. 1975. Cross-bridge conformation as revealed by x-ray diffraction studies of insect flight muscle with ATP analogues. *Biophys. J.* 15:687–705.

Henderson, R., and P. N. T. Unwin. 1975. Three-dimensional model of purple membrane obtained by electron microscopy. *Nature* (*Lond.*). 257:28–32.

Heuser, J. E. 1983. Structure of the myosin cross-bridge lattice in insect flight muscle. *J. Mol. Biol.* 169:123–154.

Holmes, K. C., R. T. Treager, and J. Barrington Leigh. 1980. Interpretation of the low angle x-ray diffraction from insect flight muscle in rigor. *Proc. R. Soc. B.* 207:13–33.

Huxley, H. E., R. M. Simmons, A. R. Faruqui, M. Kress, J. Bordas, and M. H. J. Koch. 1983. Changes in the x-ray reflections from contracting muscle during rapid mechanical transients and their structural implications. *J. Mol. Biol.* 169:469–506.

Lovell, S. J., P. J. Knight, and W. F. Harrington . 1981. Fraction of myosin heads bound to thin filaments in rigor fibrils from insect flight and vertebrate muscles. *Nature* (*Lond.*). 293:664–666.

Luther, P. K., and R. A. Crowther. 1984. Three dimensional reconstruction from tilted sections of fish muscle M-band. *Nature* (*Lond.*). 307:566–568.

Moore, P. B., H. E. Huxley, and D. J. DeRosier. 1970. Three-dimensional reconstruction of F-actin, thin filaments and decorated thin filaments. *J. Mol. Biol.* 50:279–295.

Reedy, M. K. 1968. Ultrastructure of insect flight muscle. I. Screw sense and structural grouping in the rigor cross-bridge lattice. *J. Mol. Biol.* 31:155–176.

Reedy, M. K., K. C. Holmes, and R. Tregear. 1965. Induced changes in orientation of the cross-bridges of glycerinated insect flight muscle. *Nature* (*Lond.*). 207:1276–1280.

Reedy, M. K., R. S. Goody, W. Hofmann, and G. Rosenbaum. 1983*a*. Co-ordinated electron microscopy and x-ray studies of glycerinated insect flight mucle. I. X-ray diffraction monitoring during preparation for electron microscopy of muscle fibers fixed in rigor, in ATP, and in AMPPNP. *J. Muscle Res. Cell Motil.* 4:25–53.

Reedy, M. C., M. K. Reedy, and R. S. Goody. 1983*b*. Coordinated electron microscopy and x-ray studies of glycerinated insect flight muscle. II. Electron microscopy and image reconstruction of muscle fibres fixed in rigor, in ATP, and in AMPPNP. *J. Muscle Res. Cell Motil.* 4:55–81.

Reedy, M. K., and M. C. Reedy. Rigor cross-bridge structure from flared Xes and tilt views of single filament layers in insect flight muscle. *J. Mol. Biol.* In press.

Smith, R. R., W. E. Fowler, T. D. Pollard, and U. Aebi. 1983. Structure of the actin molecule determined from electron micrographs of crystalline actin sheets with a tentative alignment of the molecule in the actin filament. *J. Mol. Biol.* 167:641–660.

Stewart, M., R. W. Kensler, and R. J. C. Levine. 1985. Three-dimensional reconstruction of thick filaments from *Limulus* and scorpion muscle. *J. Cell Biol.* In press.

Taylor, K. A., and, L. A. Amos. 1981. A new model for the geometry of the binding of myosin cross-bridges to muscle thin filaments. *J. Mol. Biol.* 147:297–324.

Taylor, K. A., M. C. Reedy, L. Cordova, and M. K. Reedy. 1984. Three-dimensional reconstruction of rigor insect flight muscle from tilted thin sections. *Nature* (*Lond.*). 310:285–291.

Thomas, D. D., R. Cooke, and V. A. Barnett. 1983. Orientation and rotational mobility of spin-labeled myosin heads in insect flight muscle in rigor. *J. Musc. Res. Cell Motil.* 4:367–378.

Thomas, D. D., and R. Cooke. 1980. Orientation of spin-labeled myosin heads in glycerinated muscle fibers. *Biophys. J.* 32:891–906.

Toyoshima, C., and T. Wakabayashi. 1985. Three-dimensional image analysis of the complex of thin filaments and myosin molecules from skeletal muscle. V. Assignment of actin in actin-tropomyosin-myosin subfragment-1 complex. *J. Biochem.* 97:245–263.

Unwin, P. N. T. 1977. Three-dimensional model of membrane-bound ribosomes obtained by electron microscopy. *Nature (Lond.)*. 269:118–122.

Unwin, P. N. T., and G. Zampighi. 1980. Structure of the junction between communicating cells. *Nature (Lond.)*. 283:545–549.

Vibert, P., and R. Craig. 1982. Three-dimensional reconstruction of thin filaments decorated with a Ca^{2+}-regulated myosin. *J. Mol. Biol.* 157:299–319.

Vibert, P., and R. Craig. 1983. Electron microscopy and image analysis of myosin filaments from scallop striated muscle. *J. Mol. Biol.* 165:303–320.

Yanagida, T. 1981. Angles of nucleotides bound to cross-bridges in glycerinated muscle fiber at various concentrations of e-ATP, e-ADP, and e-AMPPNP detected by polarized fluorescence. *J. Mol. Biol.* 146:539–560.

Wakabayashi, T., H. E. Huxley, L. A. Amos, and A. Klug. 1975. Three-dimensional image reconstruction of actin-tropomyosin complex and actin-tropomyosin-troponin T-troponin I complex. *J. Mol. Biol.* 93:477–497.

DISCUSSIONS

Session Chairman: Thomas D. Pollard.
Scribes: Robert Grant, Katherine Crumley, and Vincent Barnett.

VIBERT: What is the dimension of actin in your recent representation?

TAYLOR: In the projection map shown in Fig. 5*b*, the thin filament is 14.6 nm by 12.1 nm. It is worth pointing out, however, that the density at the actin position in the reconstruction is not due just to actin, but also has a significant contribution from attached crossbridges which give it its elliptical profile as seen in projection. Comparison of Fig. 3, which is from the original MYAC row lattice line data, unscaled, with Fig. 5*b*, which is from the MYAC row data scaled to the MYAC layer data, should give you some idea of the effect of the mass loss on the reconstruction.

POLLARD: Could you comment more extensively on the mass loss phenomenon? Presumably these proteins are embedded in plastic. Is the plastic etched away from the surface? Is there a rearrangement of proteins?

TAYLOR: Radiation damage effectively breaks the intramolecular bonds, producing highly reactive free radicals. These will rearrange themselves, producing some volatile fragments, which will be lost in the microscope vacuum. The remainder will condense into some sort of carbonaceous material, occupying a smaller volume. The heavy atom stain, which is really what we are visualizing here, can be effected because of changes in the supporting structures.

STEWART: Radiation damage is expected to occur when this sort of micrograph is taken. Are you certain that at each subsequent micrograph in the tilt series you don't have a more radiation-damaged specimin ? How would the radiation damage affect the reconstruction?

TAYLOR: Progressive mass loss over the period of time that the tilt series data are being collected would be a serious problem. We originally tried to minimize the effect by collecting first the highest tilts, which would be the most affected. We have also measured, on different areas of tilt sections, the change in inelastic electron scattering (which can be used as a measure of mass loss) as a function of time using Electron Energy Loss Spectroscopy (EELS). By this criterion the mass loss leveled off at ~ 40% of the original mass at a dose of 40,000 e/nm^2, so we believe the sections had stabilized before the first micrograph was taken.

REEDY: We had some contradictory experiences with the mass loss problem. Somewhere up to a third of the section thickness appears to have collapsed, coincident with a corresponding amount of mass loss.. This fits fairly well with the resulting reconstruction, and helps explain the discrepancy between the original and the finally corrected version. Aside from that, I've had some experience which relates to Pauline Bennet's earlier work suggesting that sections always collapse and everything in them always collapses proportionately.

In general, we prefer Araldite over Epon as an embedding medium. Consider a 120-nm thick Araldite longitudinal section containing several layers of the hexagonal filament lattice. By tilting the section through 120° you are able to observe all three equivalent 60° lattice directions, independent of the radiation dose. In Epon they would collapse and the 60° angular separation would enlarge towards 90°. In Araldite, the mass loss doesn't necessarily cause distortion of the included heavily-stained material. However, there is definitely some collapse of structure indicated in the thinner sections by the present study.

VIBERT: Ken Taylor's maps are symmetrized so the whole thing looks uniformly squashed. Is it clear that the loss is symmetrical on the top and bottom of the section, or are we in fact losing mass from the side that's exposed to the electron beam?

TAYLOR: I presume we are losing mass homogeneously throughout the entire section.

STEWART: In the case of negatively stained frog muscle thick filaments, assymetric damage would be easily recognized. We have found no evidence of inhomogeneous mass loss. I should also say that we've found something similar to what Mike Reedy was reporting. If we negatively stain in uranyl acetate, we find that our filaments are greatly compressed and we can assess this by observing the dependence of the phases of reflections on azimunthal tilt. However, if the filaments first are treated with tannic acid and then with uranyl acetate, we do not find the same amount of compression associated with radiation damage. This may be due to increased heavy metal deposition, which confers additional resilience.

LEVINE: Can you show us the results of your three-dimensional reconstruction?

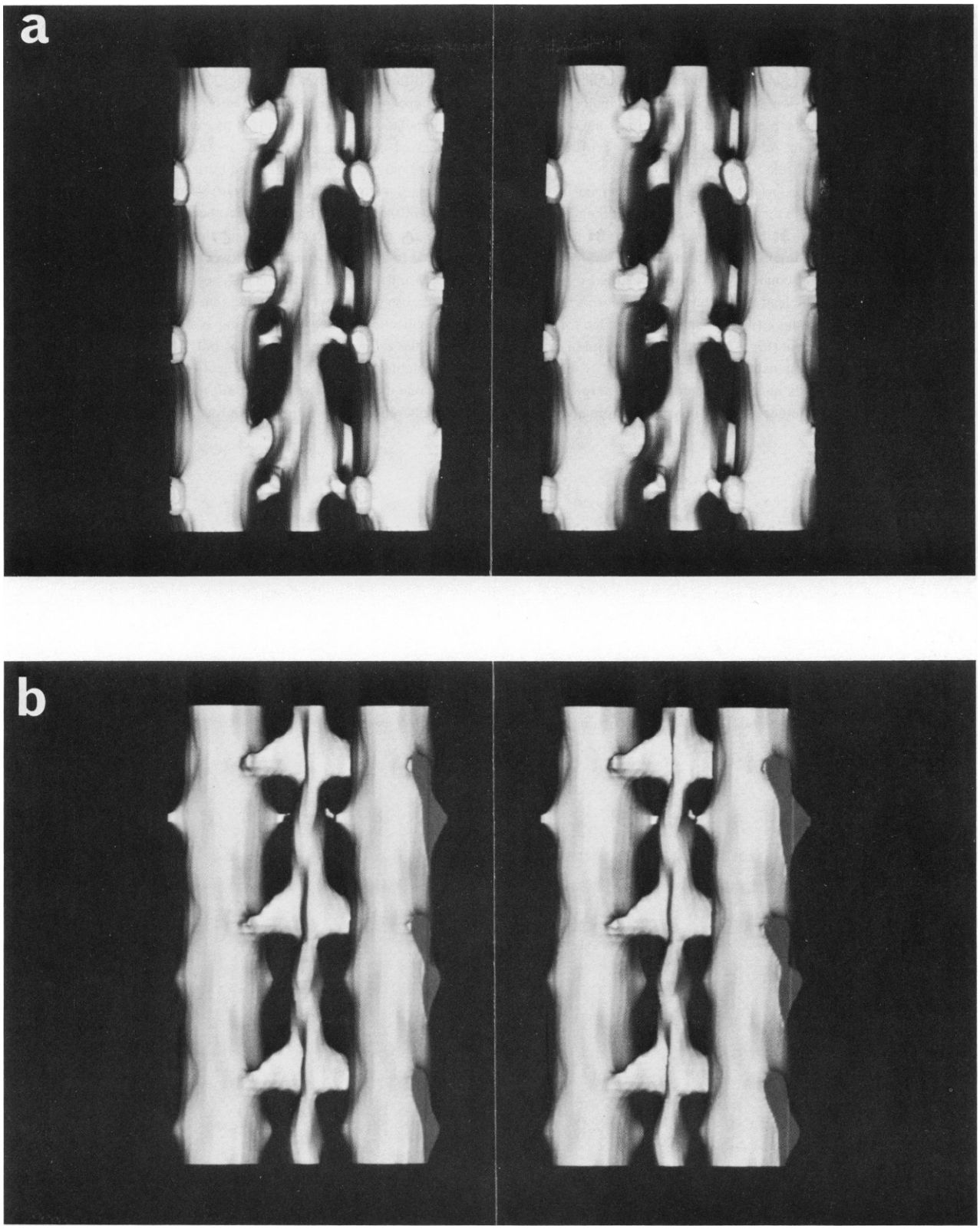

FIGURE A: Three-Dimensional Reconstruction of MYAC. Surface views of the three-dimensional reconstruction of the thin longitudinal section MYAC layer supplemented by two views derived from thick longitudinal and transverse sections and representing effectively 90° tilts of the MYAC layer about axes parallel and perpendicular to the filament axis. (*a*) View normal to the filament axis. (*b*) View of the map rotated 30° clockwise and contoured at a higher level. The stereo pair in (*a*) can be compaired directly with Fig. 3 of Taylor, et al. (1984). Note that the stereo perspective has been exaggerated in (*a*).

TAYLOR: The major effect on three-dimensional reconstructions of the missing F(0,0,Z*) data is that contrast between the features varies at different Z levels. This variation in contrast makes it difficult to choose a single contour level to represent best all the features in the map. In the reconstruction under discussion here (see Fig. A), the major effect was to make features at the surface of the reconstruction somewhat larger than they should have been. Addition of the density profile has also given them more reasonable relative sizes.

The effects of adding appropriately scaled views derived from thick sections that are orthogonal to the in-plane projection of the thin longitudinal section can be summarized as follows: Connectivity between the lead bridge and the thin filament has been improved; this is not just a contouring artifact because connectivity is now retained over a wide range of coutour levels. The lead bridge has become more triangular in shape, with a vertex on the thick filament shaft and an edge forming the connection to the thin filament (Fig A*b*). Such a shape would be consistent with two heads from a myosin molecule binding to a sihngfle thin filament. One of these heads must be oriented nearly perpendicular to the thick filament shaft; the other must be tilted at the more normal rigor angle. The length of this bridge is ~ 16 nm and has an axial extent of ~ 12 nm.

The rear bridge has been reduced in axial extent to 4.5-7.5 nm. The three different levels of the rear bridge appear quite different in size. This appears to be the primary manifestation of the 116 nm axial period; the population of myosin heads at the rear chevron is various. The axial dimension of the rear bridge is more consistent with there being on average only a single myosin head buried there.

Some density changes have occurred at the thin filament. The additional F(0,0,Z*) data has filled out the envelope of the thin filament so that a gap no longer occurs between the two strands except at very high contour levels. The separation between the two actin strands, visible in Figs. 3 and 4 of Taylor et al. (1984, see references) is decreased primarily because of the section thinning that has occurred during tilted series data collection. When this thinning is compensated in the reconstructions, the actin strand separation is only slightly changed. The changes in the actin filament long-pitch helical twist observed in the reconstruction done using only the multiple tilt views of the thin section have not been altered by the additional data.